双金属-有机框架材料衍生介孔微米棱柱状超高功率和稳定性钠离子电池负极

Bimetal-Organic-Framework Derived $CoTiO_3$ Mesoporous Micro-Prisms Anode for Superior Stable Power Sodium Ion Batteries

Zhen-Dong Huang, [†,a] Ting-Ting Zhang, [†,a] Hao Lu, [a] Jike Yang, [a] Ling Bai, [a] Yuehua Chen, [a] Xu-Sheng Yang, [b] Rui-Qing Liu, [a] Xiu-Jing Lin, [a] Yi Li, [a] Pan Li, [a] Xiao-Miao Feng, [a] and Yan-Wen Ma [a,*]

[a] *Key Laboratory for Organic Electronics & Information Displays and Institute of Advanced Materials, Nanjing University of Posts & Telecommunications, Nanjing, 210023, P. R. China.*

[b] *Advanced Manufacturing Technology Research Centre, Department of Industrial and Systems Engineering, The Hong Kong Polytechnic University, Hung Hom, Kowloon, Hong Kong, China.*

[†] Dr. Zhen-Dong Huang and Miss. Ting-Ting Zhang contributed equally to this work.

[*]Corresponding author: Y.W. Ma (iamywma@njupt.edu.cn)

Abstract: Durability, rate capability, capacity and tap density are paramount performance metrics for promising anode materials, especially for sodium ion batteries. Herein, a carbon free mesoporous $CoTiO_3$ micro-prism with a high tap density (1.8 gcm^{-3}) is newly developed by using a novel Bi-Ti-bimetal organic framework (BMOF) as precursor. It is also interesting to find that the Bi-Ti-BMOF derived carbon-free mesoporous $CoTiO_3$ micro-prisms deliver a superior stable and more powerful Na^+ storage properties than other similar reported titanias, titanates and their carbon composites. Its achieved capacity retention ratio for 1000 cycles is up to 90.3% at 5 Ag^{-1}.

1. Introduction

With the rapid expanding demand on the high rate, high energy density, long life and low cost energy storage systems for portable electronic device, electric power tools and vehicles, and storage and distribution of electric energy generated from wind, sunlight and water, massive attention have been paid to sodium ion batteries (SIBs). Compared with conventional lithium ion batteries (LIBs), SIBs are much cheaper because its earth abundance (2.74wt%) is much larger than that of Li (0.0065wt%). [1-3] However, it will be a big challenge to use metallic sodium as anode, as many serious issues, including the dendrite growth, the low Coulombic efficiency and the unstable solid electrolyte interphase caused by the intensive corrosion and active reaction of Na with electrolyte, have to been solved. [4] Before this, one of the urgent research interests for materials scientists delved into next generation SIBs is developing novel low cost anode materials with higher capacity and better cycle stability at higher power state, since the migration resistance to Na^+ is much larger than that to Li^+.

Nowadays, various advanced carbon materials have been applied as high power anode materials for SIBs, but their relatively low capacity limit the future application. [5-7] Nanostructured transition metal (Sn, Sb, etc) and their oxides or sulfides, as well as phosphours (P) and its compounds, have also attracted intensive interests because of their much higher theoretical sodium ion storage capacity. [1-3, 8] However, the poor cyclic stability due to the larger volume change is the intrinsic drawbacks as anode materials for SIBs. Lately, titanium oxides based nanostructured materials, [9-21] have been extensively studied as promising candidate anode materials due to their relatively smaller volume change than other transition metal compounds and better cyclic stability. However, their capacities and rate capability are similar or even lower than carbon anodes, which

are the main challenge for their application in both high energy and high power density type batteries. Hereby, great efforts have been made to further enhance the power and cyclic stability of titanium-based compounds by the following methods, including minimizing the particle size to increase the electrochemical reactivity of TiO_2, [9] introducing conductive carbon coating/hybrid to improve the poor electric conductivity of TiO_2, [9-12] constructing porous and hierarchical nanostructure to increase the interaction surface area between active TiO_2 and electrolyte for further enhance the rate capability of TiO_2. [13-21]

Besides the aforementioned structural and additive modification, recently, doping or incorporating with other transition metal components (N, Mo, Sn and Sb) [17-21] or directly constructing transition metal titanates (*viz*., $MTiO_3$; where M = Ni, Co, Mn) have been proposed to further promote the sodium and lithium ion storage performance of TiO_2 anodes, according to the combined intercalation and conversion reaction mechanisms. [22-26] Since the synergistic effect of TiO_2 and transition metal oxides, $MTiO_3$ exhibits a much higher theoretical capacity (500 ~ 1000 $mAhg^{-1}$ for SIBs depending on the sodium ion storage mechanism) than titanium oxides. [22-24] Some recent reports also indicate $MTiO_3$ presents much better cyclic stability than that of their transition metal based anodes. [24-26] However, there are only few works reported the sodium ion storage behaviors of $MTiO_3$ at a high charge/discharge current density at a relatively high tap density. [23, 24] Particularly, our previous results indicates the feasibility to achieve high power Na^+ storage performance by introducing plenty of grain boundary and mesopores into the dense $NiTiO_3$ mircoparticles for the fast ion transportation. [23] Brown et al. also demonstrated that the large sized $CoTiO_3$ prepared by high temperature solid state method could deliver capacity of 139 and 128 $mAhg^{-1}$ during the first and second charge at 15 mAg^{-1} in a sodium ion cell, which are

much higher than that of 19 $mAhg^{-1}$ on $MnTiO_3$ prepred by similar solid state method. [24] Moreover, $CoTiO_3$ shows much lower band gap energy (2.34 eV), larger unit cell (a=5.49 Å) and relatively lower formation temperature (~500 ^oC) than that of $NiTiO_3$ (3.02 eV, 5.44 Å, and ~550 ^oC, respectively). [23, 27] Therefore, $CoTiO_3$ should be more conductive and can provide larger space to accommendate the volume change during the sodiation process. Thus, it will be also very interesting and important to further understand and continuously promote the sodium ion storage performance. Hence, a carbon free mesoporous $CoTiO_3$ hexagonal micro-prism with a high tap density (1.8 gcm^{-3}) is developed in this work for achieving superior stable and powerful sodium ion storage capability.

2. Experimental

2.1. Raw materials

In this work, Urea (Purity≥99%, Xilong Chemical Co., Ltd.), $Co(C_2H_3O_2)_2{\cdot}4H_2O$ (Purity≥99%, Aladdin), titanium butoxide (TBO) (Purity≥98%, Aladdin), ethylene glycol (AR grade, Shanghai No.4 Reagent & H.V. Chemical Limited Company) and ethanol (Purity≥99.5%, Aladdin)were used as raw materials to prepare the Co-Ti-EG metal organic crystal precursor and the final product cobalt titanate.

2.2. Synthesis of $CoTiO_3$ mesoporous microprism

The preparation process and the colour evolution during the preparation process of $CoTiO_3$ micro-prism are shown in Fig. 1. In a typical synthesis process, the bimetal organic framework (BMOF) Co-Ti-EG was firstly prepared as a precursor using the rationally designed solvothermal reaction. First, stoichiometric amounts of urea, cobalt acetate tetrahydrate and titanium butoxide (TBO) were successively dissolved in a molar ratio of 3:1:1 into 60 ml ethylene glycol (EG) to

form a clear red solution under magnetic stirring at room temperature. Here, EG acts as both solvent and complexing agent. As shown in Fig. 1, during the magnetic stirring process, the clear red solution gradually turns to a light pink suspension. This observation indicates that EG has reacted with Ti^{4+} and Co^{2+} to form Co-Ti-EG polymer chain precursor. To further enhance the crystallinity of Co-Ti-EG BMOF, the obtained light pink suspension of Co-Ti-EG was sealed into a 100ml teflon-lined stainless steel autoclave. Subsequently, the autoclave was put into an electro-thermally blowing dry box preheated to 120 ^{o}C. After a six-hour solvothermal reaction, Co-Ti-EG BMOF was obtained by collecting and washing the solvothermal product with ethanol for 3 times. The obtained BMOF was put in a muffle furnace and calcined at a temperature ranging from 600 ^{o}C for 5 h at a heating rate of 10 ^{o}Cmin^{-1} under air to fully remove the organic component in BMOF. Finally, a highly crystalline $CoTiO_3$ green powder was obtained.

2.3. Characterization

The morphology of as-prepared precursor and the final products were characterized by using field emission scanning electron microscopy (FE-SEM, Hitachi S-4800) at an acceleration voltage of 3 kV. The optical photos were taken by digital camera. Nitrogen adsorption/desorption isotherms were obtained at 77 K using an automated adsorption apparatus (Micromerit-ics ASAP 2020). The surface area was calculated based on the Brunauer–Emmett–Teller (BET) equation. X-ray diffraction patterns of the as-prepared precursor and final products were measured on an X-ray diffractometer (RIGAKU, RINT-ULTIMA III) using Cu *K*α radiation (λ= 1.54051Å). The diffraction patterns were recorded in a 2θ range of 10-70 ^{o} with a step size of 0.01 ^{o}.

To investigate the electrochemical performance of as-prepared $CoTiO_3$ micro-prisms, the composite electrodes of the final product $CoTiO_3$ were prepared by coating their uniform slurry

mixed with acetylene black (AB) and polyvinylidenefluoride (PVDF) (active materials:AB:PVDF=75:15:10). The electrode was then pressed and punched out into 10 mm (in diameter) disks. Two-electrode sodium ion batteries were assembled in an ultrapure Ar-gas filled glove box to investigate the sodium ion storage performance of the final product $CoTiO_3$. The electrolyte used was a 1 mol L^{-1} $NaPF_6$ in ethylene carbonate (EC) + dimethyl carbonate (DMC) in a volume ratio of 1:1 with the addition of trace FEC. Sodium discs were used as counter electrodes. Cyclic voltammetry (CV) and galvanostatic charge and discharge measurements were carried out in a voltage range of 0.01 to 3 V vs Na/Na^+ at a current density ranged from 0.25 to 5 Ag^{-1}, respectively. The electrochemical impedance spectroscopy was carried out in a frequency range of 0.01Hz to 100 kHz, and the perturbation amplitude was controlled at 5 mV. The galvanostatic charge/discharge test were performed on a battery testing system (CT2001A, Wuhan Land). The aged cells were discharged/charged within the voltage window of 0.01 to 3.0 V at current densities corresponding to 0.5C, 1C, 2C, 5C and 10C rate (1C = 500mAhg^{-1}) under constant current mode.

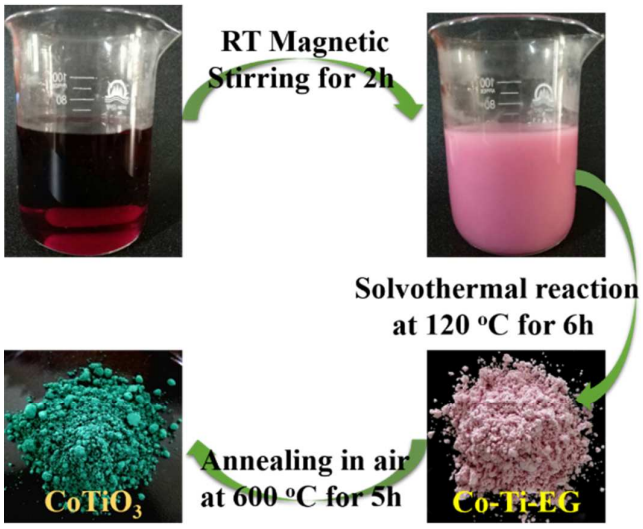

Fig. 1. The preparation and color evolution process for the preparation of mesoporous $CoTiO_3$ hexagonal micro-prisms.

3. Results and discussions

The typical preparation process and the colour evolution phenomenon of the scalable metal-organic framework (MOF) derived strategy for the desired mesoporous $CoTiO_3$ micro-prisms are clearly shown Fig. 1. At the beginning, one-dimensional (1D) Co-Ti bimetal organic frameworks (BMOF) were self-assembled by a rational modified solvothermal method. In a typical synthesis process, stoichiometric amounts of urea, cobalt acetate tetrahydrate and titanium butoxide (TBO) were firstly dissolved in a molar ratio of 3:1:1 into 60 ml ethylene glycol (EG) to form a clear red solution under magnetic stirring at room temperature. During the continuously magnetic stirring, EG gradually reacted with Ti^{4+} and Co^{2+} to form Co-Ti-EG polymer chain precursor, meanwhile the clear red solution gradually turns to a light pink suspension. After a further crystallizing treatment under solvo-thermal condition at 120 ^{o}C for 6 h in a sealed teflon-lined stainless steel, highly crystalized and well-cut hexagonal dense micro-prisms of pink Co-Ti-EG BMOF were finally obtained. As shown in Figs. 2a and 2b, the length and diameter of single Co-Ti-EG hexagonal micro-prisms are 2～4 μm and 0.5～1 μm, respectively. The well-defined X-ray diffraction (XRD) pattern, given in Fig. 3a, is similar with the reported pattern of Ni-Ti-EG BMOF, which indicates the self-assembling mechanism of the highly crystalline pink Co-Ti-EG BMOF are similar, [23] due to the close nature of Co^{2+} with Ni^{2+}.

The fourier transform infrared (FTIR) spectroscopy provided in Fig. 3b further confirm the metal-organic complex nature of Co-Ti-EG BMOF.Peaks centered at 2831 and 2931 cm^{-1} is indexed to the symmetry and anti-symmetry stretching vibration (ν_s and ν_{as}), respectively, of C–H bonding in the group of $–CH_2–$, instead of $–CH_3$. Peaks centered in

3403, 1458, 1070 and 887 cm^{-1} can be assigned to the ν_{OH}, δ_{OH}, ν_{CO} and γ_{OH} of C–O and O–H bonding in the group of $–CH_2–OH$, respectively. Moreover, the peaks centered in 2484, 1866, 1323 and 1212 cm^{-1} can be indexed to the ν_{OH}, $\nu_{C=O}$ δ_{OH}, and ν_{CO} of C=O, C–O and O–H bonding in the group of –COOH, respectively.

After being annealed at 600 ^{o}C for 5h in air, the obtained green $CoTiO_3$ powder featured obviously mesoporous structure that constructed with closely packed primary $CoTiO_3$ nanoparticles into a hexagonal mirco-prism, as shown in Figs. 2c, 2d and 4a. The primary particle size is around 50 ~ 150 nm.

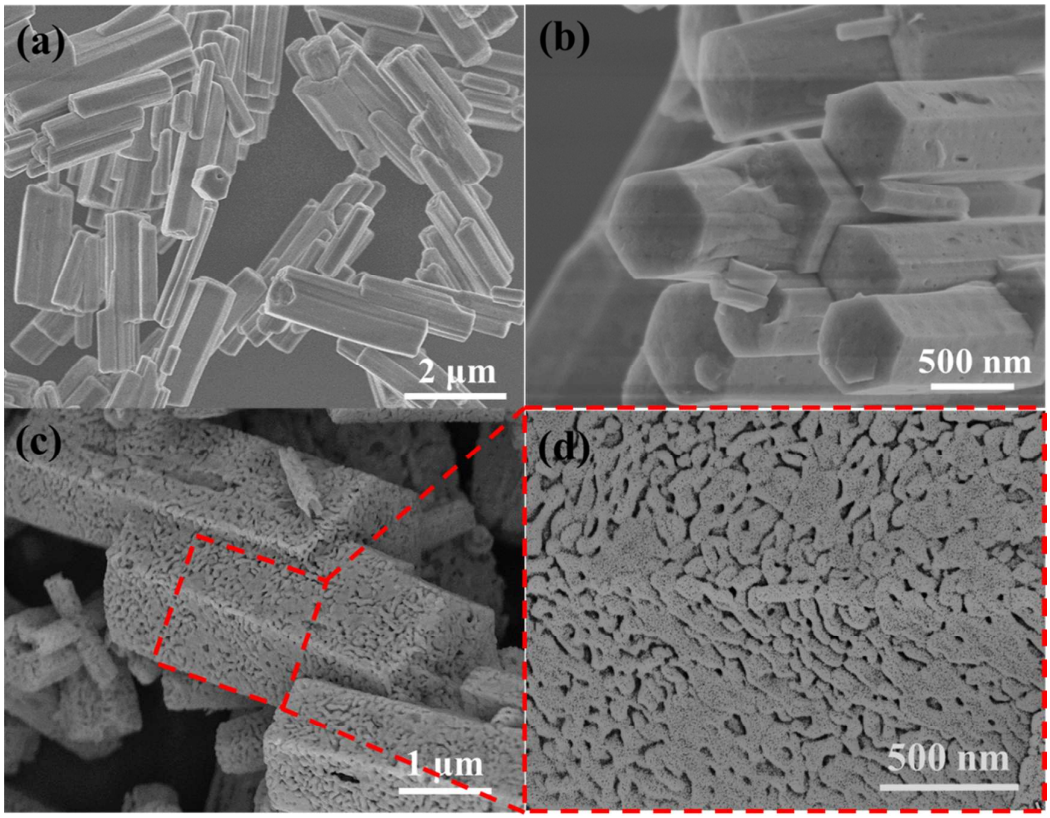

Fig. 2. (a) and (b) the SEM images of Co-Ti-EG DMOC, (c) and (d) the SEM images of $CoTiO_3$ mesoporous micro prisms.

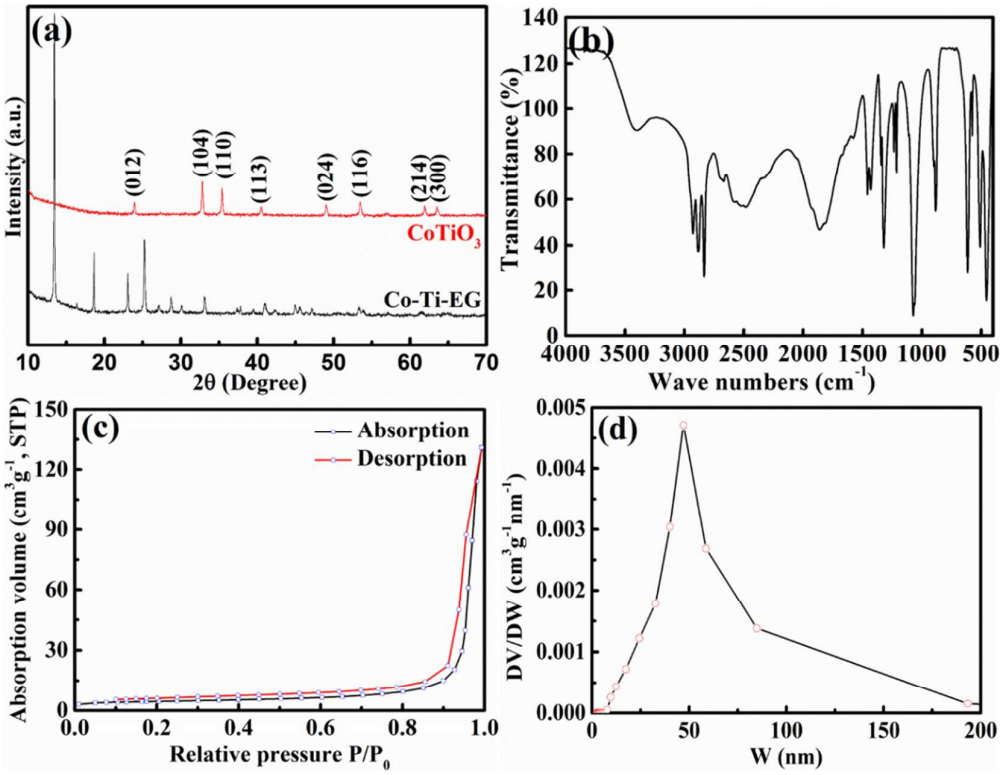

Fig. 3. (a) The XRD patterns of Co-Ti-EG and $CoTiO_3$ prisms, (b) the FTIR spectrum, (c) N_2 adsorption–desorption isotherm profile and (d) the pore size distribution curve of the as-prepared porous $CoTiO_3$ prism.

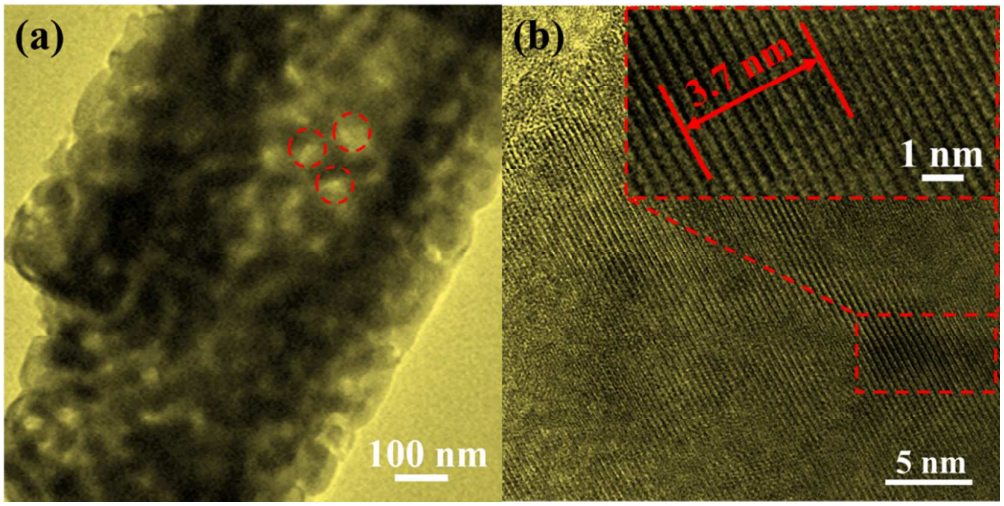

Fig. 4. (a) low and (b) high resolution TEM images of as-prepared $CoTiO_3$ mesoporous micro-prism.

The sharp XRD pattern present in Fig. 3a indicates the pure ilmenite structure. The HRTEM image in Fig. 4b corresponding to the selected area also clearly confirms the lattice fringes of the (012) (d_{012} = 0.37 nm) crystallographic planes of ilmenite $CoTiO_3$. Furthermore, the pore size is mainly 20 ~ 150 nm, average 50 nm, as clarified by the TEM images shown in Fig. 4a and the pore size distribution curve given in Fig. 3d. The BET specific surface area calculated based on the N_2 adsorption–desorption isotherm profile in Fig. 3c is about 15.6 m^2g^{-1}. The mesoporous structure can provide effective channel for the adequately infiltration of electrolyte inside the $CoTiO_3$ micro-prism to increase the efficiency and achieve high rate sodium ion transportations. Moreover, the interconnected nanoscale primary particle in turn can promote the rate performance of $CoTiO_3$ secondary micro-prisms by decreasing the solid state diffusion of sodium within the nano-size $CoTiO_3$ particles and creating large amount of disorder state interface for shortcut diffusion of Na^+ during the charge/discharge process. Considering the intrinsic low volume change during Na^+ insertion/extraction, the as-prepared mesoporous $CoTiO_3$ hexagonal micro-prisms would show desirable rate and cyclic performance, in terms of the abovementioned unique metrics.

To understand the Na^+ storage properties of $CoTiO_3$, the electrodes made of desired $CoTiO_3$ mesoporous micro-prisms were used as working electrode, metallic sodium and glass fiber membrane were used as counter/reference electrode and separator, respectively. The electrochemical performance were tested in a two-electrode setup in an electrolyte of 1 M $NaPF_6$ in ethylene carbonate (EC) + propylene carbonate (PC) in a volume ratio of 1:1 with the addition of trace amounts of fluoroethylene carbonate (FEC). The obtained sodium ion storage properties are given in Fig. 5. During initial cycling at 0.5C in sodium ion batteries, the discharge/charge capacity of $CoTiO_3$ are 551.3/161.3 $mAhg^{-1}$ at room temperature, as can be seen in the

charge/discharge voltage profiles shown in Fig. 5a. The initial coulombic efficiency is ~ 29.3%, which is comparable to mesoporous $NiTiO_3$ micro-prisms. [23] The observed initial discharge capacities, namely 551.3 $mAhg^{-1}$, are comparable to the theoretical capacity of $CoTiO_3$ (519.5 $mAhg^{-1}$) based on the following initial sodiation mechanism:

$$CoTiO_3 + 3Na^+ \rightarrow NaTiO_2 + Co + Na_2O \quad [1]$$

The slightly higher discharge capacity than theoretical value should be accounted for the formation of solid electrolyte interphase on the surface of $CoTiO_3$ nanoparticles. The low discharge capacity than reported $NiTiO_3$ should be caused by the much large particle size and much lower specific surface area, see Table 1. The probable reversible de-sodiation mechanism responsible for the charge capacity of 161.3 $mAhg^{-1}$ could be as follows:

$$NaTiO_2 + xCo + xNa_2O \rightarrow TiO_2 + xCoO + (1+2x)Na^+ \quad [2]$$

Most of the irreversible capacity should be caused by the irreversible reaction. Only partially newly formed Co and Na_2O react to CoO and Na^+. In this case, x is around 0.17. This should be one of the main reasons resulted in the low initial coulombic efficiency. The relatively large particle size and low specific surface area could be another reason responsible for the relatively lower electrochemical activity, since the sodium ion storage performance is highly affected by the increase of particle size. [10] Therefore, the obtained $CoTiO_3$ mesoporous micro-prism deliver a much higher capacity and rate performance than that of reported $CoTiO_3$ (139 $mAhg^{-1}$) synthesized by solid state method, as given in Table 1. [24] Additionally, the large irreversible conversion reaction also could be confirmed by the CV analysis results, shown in Fig. 5f. During the subsequent cycles, the electrochemical performance is gradually get stabilization, as observed from the evolution of the charge/discharge profiles and the CV curves, see Figs. 5b and 5f.

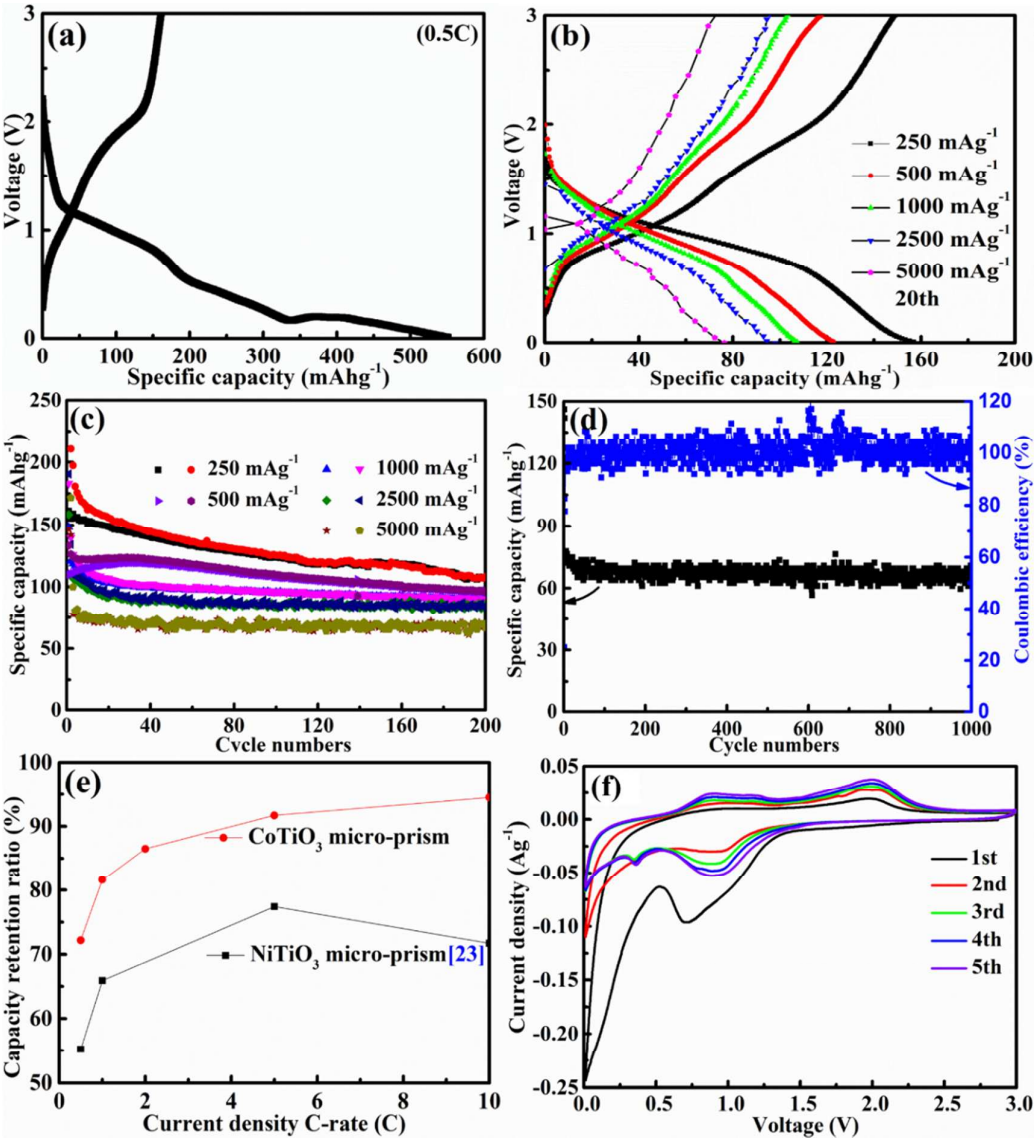

Fig.5. The electrochemical performance of the desired $CoTiO_3$ mesoporous micro-prisms anode materials: (a) the first cycle at 0.5C and (b) the 20^{th} cycle charge/discharge voltage profiles and (c) cyclic and rate capability for the as-prepared $CoTiO_3$ at a current density of 0.5C, 1C, 2C, 5C and 10C, respectively; (d) the cyclic performance and coulombic efficiency at 10C for 1000 cycles, (e) the capacity retention ratio of the as-prepared $CoTiO_3$ micro-prisms from 20^{th} to 200^{th} cycles to the reported $NiTiO_3$ micro-prisms [23]. (1C = 500 mAg^{-1}) (f) cyclic voltammetry curves at 0.1 mVs^{-1} during the initial five cycles.

As shown in Fig. 5f, three oxidation peaks (located at 0.86, 1.21 and 2.00 V, respectively) and one broad (0.90 V), should be responsible for the re-oxidation of Co and Ti^{3+} to Co^{2+} and Ti^{4+} due to the extraction of Na^{+} from the host structure. The reduction peaks located at 0.90 and 0.36 V are apparent from the second cycle. The results observed from CV test is consistent with the galvanostatic charge/discharge profiles shown in Figs. 5a and 5b, which also indicate a similar sodium storage behaviour of as-developed $CoTiO_3$ mesoporous prisms with that of $NiTiO_3$ reported in [22-24].

Interestingly, it is also glad to find from Fig. 5c that the charge capacity retention ratio of the obtained $CoTiO_3$ significantly increased from 72.2% at 0.5C to 81.6% at 1C, to 86.5% at 2C, and further increased to 91.7% at 5C, and finally increase to 94.5% at 10C, from the 20th to 200th cycle. Even after cycling at 10C for 1000 cycles, the capacity retention ratio is maintained at 90.3%, as can be seen in Fig. 5d. At the same time, the chare/discharge coulombic efficiency are around 100%. As shown in Fig. 5e, the observed capacity retention ratio of $CoTiO_3$ mesoporous micro-prisms are much higher than that of the just reported $NiTiO_3$ with similar morphology.

Based on above observation, present $CoTiO_3$ micro-prisms can provide much superior rate and excellent cyclic performance at high current density at such high tap density (1.8 gcm^{-3}). As present in Table 1, the as-prepared pure $CoTiO_3$ micro-prisms also deliver significantly higher capacity and better rate capability than typical carbon materials, [5-7] and pure TiO_2 anode materials, meanwhile, show similar or even better electrochemical performance with N, Mo, Sn doped TiO_2 and ultra-small sized TiO_2. [9-21] The better electrical conductivity of $CoTiO_3$ than $NiTiO_3$, TiO_2, because of the narrower band gap of $CoTiO_3$ (2.34 eV) than $NiTiO_3$ (3.02 eV) and TiO_2 (3.3 eV), should be one of the reason responsible for the much enhanced sodium ion storage performance.

[27, 28] Comparing to the reported counterparts, $NiTiO_3$ nanoparticle and micro-prisms, the initial capacity of $CoTiO_3$ are lower than reported $NiTiO_3$, [22, 23] however, the preserved charge capacity of $CoTiO_3$ at 10C after 1000 cycles still kept 65.3 $mAhg^{-1}$, which is much higher than 51.1 $mAhg^{-1}$ of reported $NiTiO_3$. [23] Especially at high rate, the capacity retention ratio of the reported $NiTiO_3$ at 10C is only 44.3% from the 20th to 1000th cycle, 46% lower than 90.3% achieved by as-prepared $CoTiO_3$. The larger pore size of the obtained $CoTiO_3$ mesoporous micro-prism than $NiTiO_3$ is helpful to accommodate the volume change during the (de-)sodiation process, which will be good for the improvement of cyclic stability. Therefore, all the above results indicate that the as-prepared $CoTiO_3$ mesoporous micro-prisms can be potential anode materials for superior power stable sodium ion storage, once the surface condition of $CoTiO_3$ with conductive carbon and the primary particle size, the quality of the electrolyte and battery assembly process are properly optimized.

Table 1. A comprehensive comparison of the sodium ion storage properties of present $CoTiO_3$ mesoporous micro-prism, reported $NiTiO_3$ and TiO_2-based nanostructured anode materials.

No	Materials and Morphology	PP / SP* size	Low rate capacity ($mAhg^{-1}$)	High rate capacity ($mAhg^{-1}$)	High rate stability (%)	Refs. No
1	$CoTiO_3$ Mesoporous hexagonal micro-prism	50 ~ 150 nm / L: 2～4 μm, D: 0.5～1 μm, 15.6 m^2g^{-1}	161 (250 mAg^{-1})	72.3 (5 Ag^{-1})	90.3 (1000 cycle, 5 Ag^{-1})	Present work
2	$CoTiO_3$ Prepared by solid state method	/	139 (250 mAg^{-1})	/	/	[24]

3	$NiTiO_3$ nanoparticles	3 ~ 5 nm /	~400 ($250\ mAg^{-1}$)	192 ($4\ Ag^{-1}$)	88.4 (200 cycle, $0.5\ Ag^{-1}$)	
4	$NiTiO_3$ Mesoporous hexagonal micro-prism	30 ~ 100 nm / L: 2～4 μm, D: 0.5～1 μm, 30 m^2g^{-1}	278 ($250\ mAg^{-1}$)	118 ($5\ Ag^{-1}$)	44.3 (1000 cycle, $5\ Ag^{-1}$)	[23]
5	Anatase C-coated TiO_2 nanoparticles	40 nm / 11 nm /	~135 ($335mAg^{-1}$) 195	50 ($3.35\ Ag^{-1}$) 135	/ /	[10]
6	Graphene-Rich Wrapped Petal-Like Rutile TiO_2 tuned by Carbon Dots	~10 nm / D: ~300 nm	~185 ($167\ mAg^{-1}$)	59.8 ($4.2\ Ag^{-1}$)	100 (1000 cycles $3.35\ Ag^{-1}$)	[11]
7	Anatase TiO_2 nanopores	~20 nm/ 55.573 m^2g^{-1}	~164.3 ($167\ mAg^{-1}$)	46.4 ($3.35\ Ag^{-1}$)	102.6 (200 cycles $0.84\ Ag^{-1}$)	[14]
8	Mo-doped anatase TiO_2	/	~162.4 ($167\ mAg^{-1}$)	~109.5 ($1.67\ Ag^{-1}$)	109.2 (100 cycles $0.03\ Ag^{-1}$)	[20]
9	anatase TiO_2	/	~89.6 ($167\ mAg^{-1}$)	~43.9 ($1.67\ Ag^{-1}$)	108.8 (100 cycles $0.03\ Ag^{-1}$)	[20]
10	Olive-like TiO_2 coated with carbon	/80 nm /150 nm	~225 ($167\ mAg^{-1}$) ~202	~105 ($6.7\ Ag^{-1}$) ~75	94.6 (1000 cycles $3.36\ Ag^{-1}$) 96.1	[9]
11	N_2-doped mesoporous TiO_2 nanofiber	25 nm / D: 500 nm	220 ($336\ mAg^{-1}$)	~108 ($3.36\ Ag^{-1}$)	94.0 (500 cycles $3.36\ Ag^{-1}$)	[17]
12	mesoporous TiO_2 nanofiber	25 nm / D: 500 nm	173 ($336\ mAg^{-1}$)	~87 ($3.36\ Ag^{-1}$)	94.3 (500 cycles	[17]

					3.36 Ag^{-1})	
	Carbon-coated	10 ~ 50 nm/	~130.6	~70.6	99	
13	rutile titanium		(336 mAg^{-1})	(3.36 Ag^{-1})	(500 cycles	[12]
	dioxide				3.36 Ag^{-1})	
14	Rutile titanium	10 ~ 50 nm/	~55	~22.6	/	[12]
	dioxide		(336 mAg^{-1})	(3.36 Ag^{-1})		

PP : primary particle / SP: secondary particle

4. Conclusions

In this paper, a bimetal organic framework (BMOF)-derived mesoporous $CoTiO_3$ micro-prisms was prepared as potential anode materials for superior power and cyclic stable sodium ion storage. The as-prepared $CoTiO_3$ shows unique characteristics, including the mesoporous structure formed by the interconnection of nano-size primary $CoTiO_3$ particle, the relatively high tap density (1.8 gcm^{-3}) hexagonal 1D micro-prism formed by close-packing nano-size primary $CoTiO_3$ particle, relatively higher conductivity and the small volume change during the discharge/charge process. All characteristics endow the obtained nanostructured $CoTiO_3$ micro-prism with following superior rate and cyclic performance. From the 20th to the 200th cycle, the corresponding charge capacity retention ratio are 72.2%, 81.6% , 86.5% , 91.7%, and finally increase to 94.5% at 0.5C, 1C, 2C, 5C and 10C ,respectively. Even after cycling at 10C for 1000 cycles, the capacity retention ratio is maintained at 90.3%. Coupled with the scalable preparation method, the superior sodium ion storage performance brings to the fore mesoporous $CoTiO_3$ hexagonal micro-prism as a contender anode for long durability and high power sodium ion batteries.

Acknowledgements

§This work was supported by National Natural Science Foundation of China (51402155, 21373107), Priority Academic Program Development of Jiangsu Higher Education Institutions (PAPD) (YX03002), Jiangsu National Synergistic Innovation Center for Advanced Materials (SICAM), Foundation of NJUPT (NY217077), PolyU Start-up Fund for New Recruits (No. 1-ZE8R).

References

1 Xiao Y, Lee SH, and Sun YK, The Application of Metal Sulfides in Sodium Ion Batteries, Adv. Energy Mater. 2017, 7: 1601329.

2 Kang W, Wang Y and Xu J, Recent progress in layered metal dichalcogenide nanostructures as electrodes for high-performance sodium-ion batteries, J. Mater. Chem. A, 2017, 5: 7667-7690.

3 Lao MM, Zhang Y, Luo WB, Yan QY, Sun WP,and Dou SX, Alloy-Based Anode Materials toward Advanced Sodium-Ion Batteries, Adv. Mater. 2017, DOI: 10.1002/adma.201700622.

4 Zhao Y, Goncharova LV, Zhang Q, Kaghazchi P, Sun Q, Lushington A, Wang BQ, Li RYand Sun XL, Inorganic−Organic Coating via Molecular Layer Deposition Enables Long Life Sodium Metal Anode, Nano Lett., 2017, DOI: 10.1021/acs.nanolett.7b02464.

5 Chen TQ, Liu Y, Pan LK, Lu T, Yao YF, Sun Z, Chua DHC and Chen Q, Electrospun carbon nanofibers as anode materials for sodium ion batteries with excellent cycle performance, J. Mater. Chem. A, 2014, 2: 4117–4121.

6 Xiao LF, Cao YL, Henderson WA, Sushko ML, Shao YY, Xiao J, Wang W, Engelhard MH, Nie ZM and Liu J, Hard carbon nanoparticles as high-capacity, high-stability anodic materials for Na-ion batteries, Nano Energy, 2016, 19: 279–288.

7 Li ZF, Bommier C, Chong ZS, Jian ZL, Surta TW, Wang XF, Xing Z, Neuefeind JC, Stickle WF, Dolgos M, Greaney PA, and Ji XL, Mechanism of Na-Ion Storage in Hard Carbon Anodes Revealed by Heteroatom Doping, Adv. Energy Mater. 2017, DOI: 10.1002/aenm.201602894.

8 Rahman MM, Glushenkov AM, Ramireddy T and Chen Y, Electrochemical Investigation of Sodium Reactivity with Nanostructured Co_3O_4 for Sodium-Ion Batteries, Chem. Commun., 2014, 50: 5057–5060.

9 Chen J, Zhang Y, Zou GQ, Huang ZD, Li SM, Liao HX, Wang JF, Hou HS and Ji XB, Size-Tunable Olive-Like Anatase TiO_2 Coated with Carbon as Superior Anode for Sodium-Ion Batteries, Small, 2016, 12: 5554–5563.

10 Tahir MN, Oschmann B, Buchholz D, Dou XW, Lieberwirth I, Panthöfer M, Tremel W, Zentel R, and Passerini S, Extraordinary Performance of Carbon-Coated Anatase TiO_2 as Sodium-Ion Anode, Adv. Energy Mater. 2016, 6: 1501489.

11 Zhang Y, Foster CW, Banks CE, Shao LD, Hou HS, Zou GQ, Chen J, Huang ZD and Ji XB, Graphene-Rich Wrapped Petal-Like Rutile TiO_2 tuned by Carbon Dots for High-Performance Sodium Storage, Adv. Mater., 2016, 28: 9391–9399.

12 Zou GQ, Chen J, Zhang Y, Wang C, Huang ZD, Li SM, Liao HX, Wang JF, Ji XB, Carbon-coated rutile titanium dioxide derived from titanium-metal organic framework with enhanced sodium storage behavior, J. Power Sources, 2016, 325: 25–34.

13 Zhang WF, Lan TB, Ding TL, Wu NL, Wei MD, Carbon coated anatase TiO_2 mesocrystals enabling ultrastable and robust sodium storage, J. Power Sources, 2017, 359, 64–70.

14 Li SM, Xie LL, Hou HS, Liao HX, Huang ZD, Qiu XQ, Ji XB, Alternating voltage induced ordered anatase TiO_2 nanopores: An electrochemical investigation of sodium storage, J. Power Sources, 2016, 336: 196-202.

15 Hong KJ, Kim SO, Atomic layer deposition assisted sacrificial template synthesis of mesoporous TiO_2 electrode for high performance lithium ion battery anodes, Energy Storage Materials, 2016, 2: 27-34.

16 Cui ZH, Li C.L, Yu PF, Yang MH, Guo XX, and Yin CL, Reaction Pathway and Wiring Network Dependent Li/Na Storage of Micro-Sized Conversion Anode with Mesoporosity and Metallic Conductivity, J. Mater. Chem. A, 2015, 3: 509-514.

17 Wu Y, Liu XW, Yang ZZ, Gu L, and Yu Y, Nitrogen-Doped Ordered Mesoporous Anatase TiO_2 Nanofibers as Anode Materials for High Performance Sodium-Ion Batteries, Small, 2016, 12: 3522–3529.

18 Wang NN, Bai ZC, Qian YT, and Yang J, Double-Walled Sb@TiO_{2-x} Nanotubes as a Superior High-Rate and Ultralong-Life span Anode Material for Na-Ion and Li-Ion Batteries, Adv. Mater., 2016, 28: 4126–4133.

19 Yan D, Yu CY, Bai Y, Zhang WF, Chen TT, Hu BW, Sun Z and Pan LK, Sn-doped TiO_2 nanotubes as superior anode materials for sodium ion batteries, Chem. Commun., 2015, 51: 8261−8264.

20 Liao HX, Xie LL, Zhang Y, Qiu XQ, Li SM, Huang ZD, Hou HS, Ji XB, Mo-doped Gray Anatase TiO_2: Lattice Expansion for Enhanced Sodium Storage, Electrochimica Acta, 2016, 219: 227–234.

21 He HN, Wang HY, Sun D, Shao MH, Huang XB, Tang YG, N-doped rutile TiO_2/C with significantly enhanced Na storage capacity for Na-ion batteries, Electrochimica Acta, 2017, 236: 43–52.

22 Kalubarme RS, Inamdar AI, Bhange DS, Im H, Gosavi SW and Park CJ, Nickel-titanium oxide as a novel anode material for rechargeable sodium-ion batteries, J. Mater. Chem. A, 2016, 4: 17419–17430.

23 Huang ZD, Zhang TT, Lu H, Masese T, Yamamoto K, Liu RQ, Lin XJ, Feng XM, Liu XM, Wang D, Uchimoto Y and Ma YW, Grain-boundary-rich Mesoporous $NiTiO_3$ Micro-Prism as High Tap-Density, Super Rate and Long Life Anode for Sodium and Lithium Ion Batteries, Energy Storage Materials, 2017, https://doi.org/10.1016/j.ensm.2017.08.012.

24 Brown ZL, Smith S and Obrovac MN, Mixed Transition Metal Titanate and Vanadate Negative Electrode Materials for Na-Ion Batteries, J. Electrochem. Soc., 2015, 162: A15-A20.

25 Guo SM, Liu JR, Qiu S, Liu W, Wang YR, Wu NN, Guo J and Guo ZH, Porous ternary TiO_2/$MnTiO_3$@C hybrid microspheres as anode materials with enhanced electrochemical performances, J. Mater. Chem. A, 2015, 3: 23895–23904.

26 Bai X, Li T, Zhao XY, Shen D, Lun N, Qi YX and Bai YJ, Al_2O_3-modified Ti–Mn–O nanocomposite coated with nitrogen-doped carbon as anode material for high power lithium-ion battery, RSC Adv., 2016, 6: 40953–40961.

27 Lin YJ, Chang YH, Yang WD, Tsai BS, Synthesis and characterization of ilmenite $NiTiO_3$ and $CoTiO_3$ prepared by a modified Pechini method, J. Non-Crystal. Solids, 2006, 352: 789–794.

28 Acharya T, Choudhary R.N.P., Structural, dielectric and impedance characteristics of $CoTiO_3$, Mater. Chem. Phys., 2016, 177: 131-139.